A ROADMAP TO FABRICATE GEOMETRICALLY ACCURATE 3D SCAFFOLDS CO-PRINTED BY NATURAL AND SYNTHETIC POLYMERS

Connor Quigley
Sustainable Product Design and Architecture
Keene State College
229 Main St, Keene, NH-03435
Connor.quigley@keene.edu

Slesha Tuladhar
Sustainable Product Design and Architecture
Keene State College
229 Main St, Keene, NH-03435
Slesha.tuladhar@keene.edu

Ahasan Habib[1], Ph.D.
Sustainable Product Design and Architecture
Keene State College
229 Main St, Keene, NH-03435
md.ahasan.habib@keene.edu

ABSTRACT

3D bioprinting is a promising field in regenerating patient-specific tissues and organs due to its inherent capability of releasing biocompatible materials encapsulating living cells in a predefined location. Due to the diverse characteristics of tissues and organs in terms of microstructures and cell types, a multi-nozzle extrusion-based 3D bioprinting system has gained popularity. The investigations on interactions between various biomaterials and cell-to-material can provide relevant information about the scaffold geometry, cell viability, and proliferation. Natural hydrogels are frequently used in bioprinting materials because of their

[1] Corresponding author information can be added as a footnote.

high-water content and biocompatibility. However, the dominancy of liquid characteristics of only-hydrogel materials makes the printing process challenging. Polycaprolactone (PCL) is the most frequently used synthetic biopolymer. It can provide mechanical integrity to achieve dimensionally accurate fabricated scaffolds, especially for hard tissues such as bone and cartilage scaffolds. In this paper, we explored various multi-material bioprinting strategies with our recently proposed bio-inks and PCL intending to achieve dimensional accuracy and mechanical aspects. Various strategies were followed to co-print natural and synthetic biopolymers and interactions were analyzed between them. Printability of pure PCL with various molecular weights was optimized with respect to different process parameters such as nozzle temperature, printing pressure, printing speed, porosity, and bed temperature to co-print with natural hydrogels. The relationship between the rheological properties and shape fidelity of natural polymers was investigated with a set of printing strategies during co-printing with PCL. The successful application of this research can help achieve dimensionally accurate scaffolds.

INTRODUCTION

Three-dimensional (3D) bioprinting is a promising technique for the precise fabrication of scaffolds derived from reverse engineerings such as computer tomography and magnetic resonance image and computer-aided design. It can mimic the tissue and organ geometries closely ensuring the external and internal architecture of the fabricated scaffolds [1, 2]. While laser, drop-on-demand, and extrusion-based 3D bioprinting techniques are common, the latter is used frequently due to its ability to use a diverse range of natural and synthetic biopolymers and compositions [5, 6]. Natural hydrogels offer an artificial microenvironment with a higher percentage of water content that mimics the host tissue's native extracellular matrix (ECM), leading a successful tissue regeneration [3]. However, using a single type of natural polymer may not achieve the goal of ensuring the geometric fidelity of the fabricated scaffolds due to the lack of its required rheological and mechanical properties [4, 5]. Therefore, compositing various materials together is becoming popular. As a part of that effort, combining natural and synthetic polymers may contribute to the scaffold's cellular and mechanical aspects [6]. A common synthetic biomaterial, poly($\boldsymbol{\varepsilon}$-caprolactone) (PCL) is used along with natural hybrid hydrogels as a support material to ensure the geometric fidelity during the fabrication of a large scaffold, [7].

Some characteristics such as biodegradability, ease-of-manipulation, biocompatibility, stability, and U.S. Food and Drug (FDA) approval making PCL one of the frequently used synthetic polymers [8, 9]. However, it is challenging to use PCL as a single

material to regenerate tissue due to its hydrophobic and non-osteogenic natures which lead to reduced cell adhesion and bioactivity during implementation [10]. Therefore, PCL has been used with other natural biopolymers such as alginate, gelatin methacrylate (GelMA), and collagen polymers to extract the advantages of the scaffold's cellular and mechanical aspects [11].

A cell printing technique with an intention to achieve enough mechanical strength with alginate and PCL was reported [12]. Melt-plotting system was used to fabricate the scaffold with PCL and alginate powder and later cell-encapsulated alginate was printed later that scaffold. Average filament diameter and pore size were reported as 503 µm and 532 µm respectively. As a potential way for nasal reconstruction, 20% (w/v) GelMA was used with PCL encapsulating chondrocyte cells [13]. In this work, PCL was used a supporting structure (8 layers) where GelMA was printed (4 layers) in between of PCL strands to increase the build height and overall mechanical strength of the scaffolds. Young's Modulus of the scaffold fabricated with PCL/GelMA increased up to 28 MPa compared to 0.75 MPa for the scaffold fabricated with pure GelMA. PCL and nano hydroxyapatite (30%, w/v) were synthesized with melt-blending, powder blending, liquid solvent, and solid solvent techniques to explore the printability where melt-blending stood high to provide better uniformity, lowest swelling and degradation [14]. Filament diameter varies from 0.478 to 0.544 mm with various uniformity. Recently, a work has been published where scaffolds were fabricated using pure PCL and alginate-gelatin hydrogel-fill PCL following various toolpath pattern and compared the mechanical properties of those scaffolds [15]. Printing temperature 140^0C and 90^0 filament angle

showed better mechanical properties with viability of seeded cells. It was reported that the porosity of the scaffold fabricated with hydrogel-fill PCL decreased to 50% compared to the porosity of 75% of the scaffold fabricated with pure PCL. The pore size and geometries of the scaffold fabricated with hydrogel-fill PCL were not demonstrated. Therefore, we identified fabrication of various freeform structures with PCL and hydrogel materials and shape fidelity with numerical analysis were not explored extensively into those works.

Our recently proposed novel bio-inks composed of alginate-Carboxymethyl Cellulose (CMC) [16], alginate-CMC-Montmorillonite nano-clay [17], alginate-CMC-Tempo mediated Nano fibrillated Cellulose (TO-NFC) [18] showed a good the capability to ensure the geometric fidelity and cellular viability. In this paper, we will explore various multi-material bioprinting strategies with our recently proposed bio-inks [16, 18, 19] and PCL to achieve better printability and mechanical aspects. PCL with a specific molecular weight will be optimized in terms of filament width and bilayer scaffold fabrications with respect to different process parameters such as bed temperature, nozzle temperature, and applied pressure. Then, our hybrid hydrogels will be co-printed with PCL following various strategies such as depositing hybrid hydrogels on PCL base, depositing hybrid hydrogels and PCL alternatively, and depositing PCL as an outer shell and hybrid hydrogels as infill as shown in Figure 2. Printed scaffolds will be analyzed in terms of shape fidelity. Finally, a set of scaffolds will be fabricated with our hybrid hydrogels and PCL to demonstrate the capabilities of fabricating large scaffolds. 3D printing of a complex and spatially controlled heterogeneous 3D scaffold encapsulating various cell lines allows a sufficient supply of

growth factors and helps develop biomimetic scaffolds capable of replicating the patient-specific porosity and eventually tissue regeneration [20].

MATERIALS AND METHODS

Preparing materials

Polycaprolactone (PCL) pellets with three different molecular weights (Type A: Mn 45000, Type B: Mn 50000, and Type C: Mn 80,000) were used and optimized. Type B was purchased from CELLINK (CELLINK, Boston, MA), and Type A and C were purchased from Sigma Aldrich (Sigma-Aldrich, St. Louis, MO, USA). Alginate (A) and CarboxyMethyl Cellulose (CMC) were purchased from Sigma Aldrich. Tempo Mediated Nano Fibrillated Cellulose (TO- NFC) was purchased from the Process Development Center of the University of Maine (Orono, ME). In our previous work, we maintained a constant percentage of alginate (4%) with a variable percentage of CMC (1, 2, 3, and 4%) and demonstrated that CMC has a significant influence on the overall viscosity of the hybrid hydrogels [12]. In this paper, we chose three hybrid hydrogels and defined them as; Type I: 4% Alginate-4% CMC, Type II: 2% Alginate-6% CMC, and Type III: 2% Alginate-2% CMC-1% TONFC and were prepared using the protocols that published earlier [16, 18, 21]. As Type IV hydrogel, CELLINK star material (pH: 6.50-6.95) was used.

Flow behavior analysis of hybrid hydrogels

A steady rate sweep test was conducted to determine the flow behavior using a rotational rheometer (MCR 102, Anton Paar, Graz, Austria) having a parallel plate geometry (25.0 mm flat plate) setup. The plate-to-plate gap was maintained at 1.0 mm, and all data were recorded at room temperature (25°C). For flow analysis, specifically to

determine viscosity and shear stress, a variable shear strain rate from 1.0 to 100 s^{-1} was used.

3D printing

A BioX (CELLINK, Boston, MA), three-axis multi-head 3D bioprinter, was used to fabricate scaffolds. An amount of 4 ml PCL pellets was loaded into a 10.0 ml BioX thermoplastic extruder cartridge (CELLINK, Boston, MA) and heated to 100-200°C. All PCL prints utilized a nozzle having a 0.4 mm diameter. We used a range of bed temperature from 35^0C to 40^0C, porosity from 25-28%, and printing speed from 2-5mm/s. PCL having high molecular weight i.e., Mn 80,000 was extruded at a pressure of 320-380 kPa and a temperature of 170-200° C. A 3.0 ml disposable syringe was used to extrude hybrid hydrogel materials. Various process parameters such as 7-60 kPa air pressure, 250 µm disposal nozzle, 4 mm/s print speed, and 32^0C temperature were used to deposit hybrid hydrogels unless otherwise stated. Solidworks 2021 (https://www.solidworks.com), a Computer-Aided Design (CAD) software was used to design and define the vectorized toolpath of a scaffold. Slicer (https://www.slicer.org), a G-code generator software was used to generate a Bio-X compatible file including the toolpath coordinates and all process parameters to construct the scaffold. The overall scaffold fabrication process is schematically shown in Figure 1.

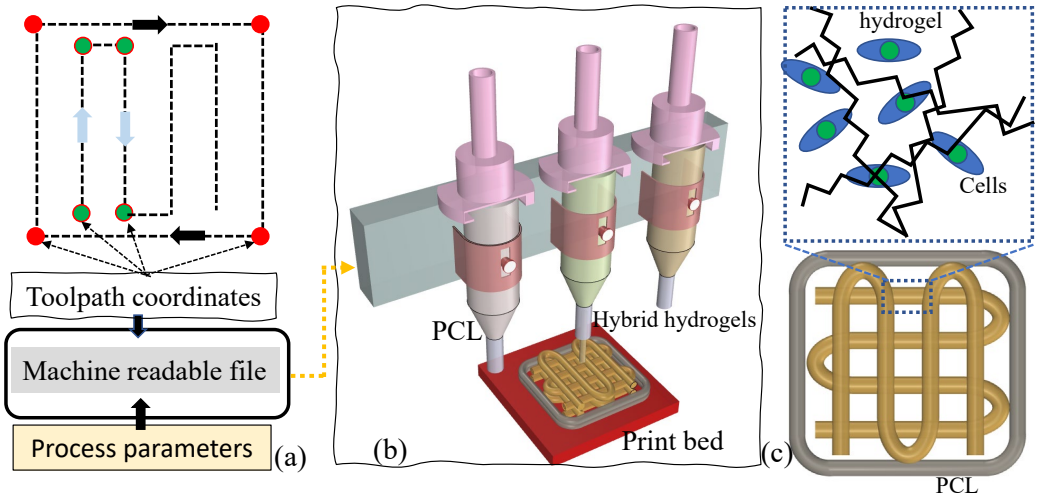

Figure 1:(a) Machine-readable file generation for multi-materials 3D bioprinting, (b) Execution of 3D bioprinting, and (c) Fabricated multi-material scaffold encapsulating living cells.

The deposition of the PCL/Hydrogel scaffolds utilized the bioprinter's multi-material alternating layer settings. These settings allow for layers, and the infill of a layer to be deposed as different materials. Generally, this setting does not include dedicated dwell times between printhead changes. However, the molecular weight of PCL and viscosity of the hydrogels used can dictate dwell time. For an example, PCL with higher molecular weight and hydrogel with lower viscosity may demand more dwell time than the opposite scenario. In this paper, we intentionally deposited high viscous hydrogels after 5 second of PCL deposition to eliminate overall wait time. The bi-material model was achieved with the authors' defined G-code edits, where tool changes were added in. No dwell time was incorporated in this process as well. The time in between tool changes, from the PCL print head to the Syringe print head, where no material deposition occurred, took approximately 5 seconds per change.

Shape fidelity

Filament released through the nozzle in an extrusion-based 3D printing system should demonstrate a constant width which will subsequently create regular grids and square holes. Normally, synthetic biopolymers such as PCL, PLA [22], and PEG [23] ensure better shape fidelity. However, a natural hydrogel with dominating liquid-like state may diffuse the deposited filament and create a circular hole for bi-layer geometry. Printability was determined using the following equation:

$$P_r = \frac{\pi}{4}\frac{1}{C} = \frac{L^2}{16A_a} \quad (1)$$

Where circularity, $C = 4\pi A_a/L^2$, L and A_a are the perimeter and actual area respectively of the pore generated by the bilayer. The under gelation ($P_r < 1$), ideal gelation ($P_r = 1$), and over gelation ($P_r > 1$) can be defined using the P_r value. The objective of determining printability is to identify the shape-holding capacity of the deposited material.

The objective of diffusion tests it to analyze the shape holding capacity of the deposited filament. The prepared hybrid hydrogels were deposited for diffusion tests, and images were captured using the CK Olympus bright field microscope (Tokyo, Japan) and analyzed using ImageJ software. The diffusion rate was determined using the following Equation:

$$d_r = \frac{A_a}{A_t} \times 100\% \quad (2)$$

Where, A_a and A_t are the actual or diffused and theoretical pore areas of the scaffold respectively. The d_r value close to 100% means the pore was not diffused due to the fusion of hydrogel meaning it has higher chance to maintain shape fidelity. On the other hand,

d_r value close to zero means the area of pore of fabricated scaffold was not identified, and it has less chance to hold the defined scaffold geometry.

Printing strategies

PCL with various molecular weights was optimized with respect to printing temperature and applied pressure in terms of printability and shape fidelity to use it with hybrid hydrogels as shown in Figure 2. We designed a scaffold having variational pore sizes to identify the shape-holding capacity of the scaffolds fabricated with optimized PCL, PCL/Type I, PCL/Type II, and PCL/Type III material as shown in Figure 2(a). We printed scaffolds having various internal features as shown in Figure 2(b) using optimized PCL, Type I, Type II, and Type III hydrogels simultaneously to see the overall interactions of those materials. Some other scaffolds shown in Figure 2 (c-f) will also be fabricated throughout this paper and will be discussed accordingly. Furthermore, a set of scaffolds was fabricated using optimized PCL and Type IV hydrogels following four different scenarios shown in Figure 3:

- Depositing six layers of PCL and four layers of Type IV hydrogels afterward.
- Deposition PCL and Type IV hydrogel alternatively until 10 layers.
- Depositing PCL as outside surface and Type IV hydrogel as infill.

Pore and filament images were captured using the CK Olympus bright field microscope (Tokyo, Japan) and analyzed using ImageJ software.

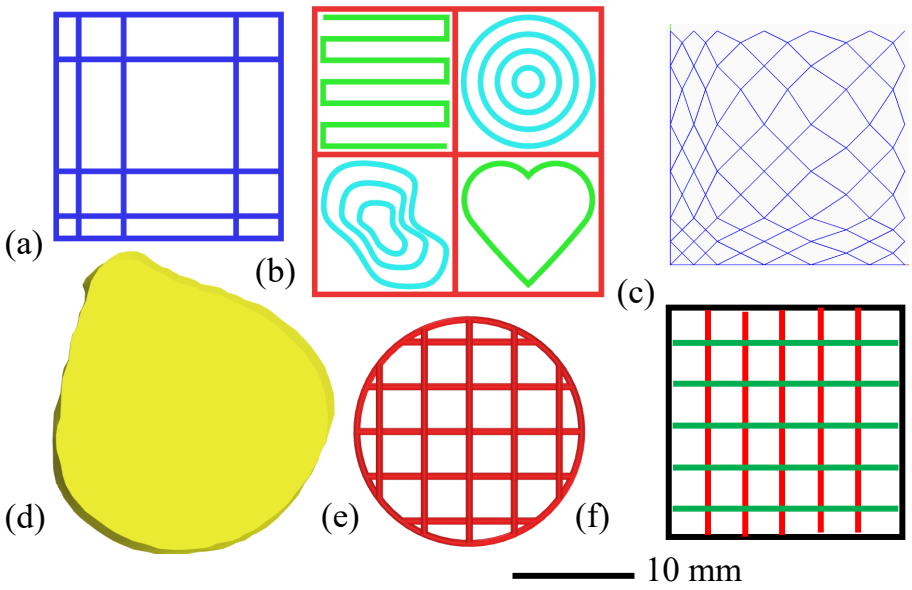

Figure 2: Various scaffolds will be fabricated throughout this paper and will be discussed accordingly. Length × width: (a,c,e,f) 20 mm×20mm, (b) 26mm×26mm, and (d) 25.07mm×27.26mm.

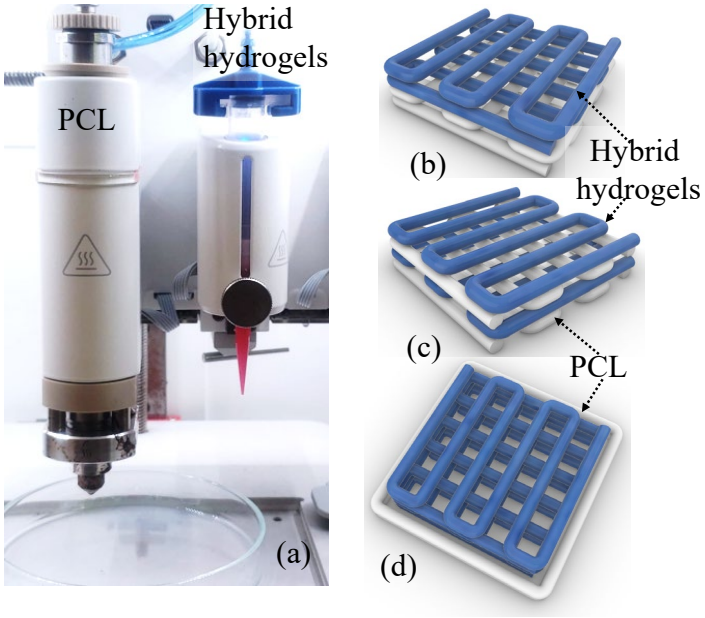

Figure 3: (a) 3D bioprinter having nozzles for extruding PCL (white color) and hybrid hydrogel (blue color). Various strategies to co-print PCL and hybrid hydrogels: (b)

depositing hybrid hydrogels on PCL base, (c) depositing hybrid hydrogels and PCL alternatively, and (d) depositing PCL as an outer shell and hybrid hydrogels as infill.

Mechanical test

The stress-strain diagram of the fabricated dog bone scaffolds (ASTM D638, n=3) was determined by uniaxial tensile force with a universal testing machine (UTM, ADMET, eXpert 2610, USA) at room temperature. A tensile force was applied at a displacement rate of 0.8 mm per second with an increment of 0.012 mm. To determine the compressive stress, some protocols from recently published works were closely followed [15, 24]. In short, scaffolds (n=4) having dimensions of 17x17x4 mm^3 were fabricated. A compression force was applied at a displacement rate of 1.3 mm per minute with an increment of 0.012 mm until 3000 N was reached.

Statistics

The data are presented as a mean ± standard deviation. The evaluation of the statistical significance of the difference of various factors is conducted at a significance level of p = 0.05 with a two-way ANOVA. Statistical software Origin Pro 5.0 was used to perform the quantitative and graphical analysis.

RESULT AND DISCUSSION

Optimization of PCL pallets

In this paper, we acquired materials from various sources with different molecular weights. A scaffold having a dimension of 20mm × 20mm × 3mm was fabricated with

various printing process parameters as shown in Figure 4. For PCL Type A, we did not get repeatable pore geometry, inter-layer morphology (inset), sharp corner, and eventually a good 3D scaffold. The nozzle temperature close to 100^0C did not help maintaining the pore size and geometry, and eventually the quality of those scaffolds as shown in Figure 4 for Type A PCL. Increasing temperature up to 120^0C seemed to improve the print quality for both scaffolds printed with applied pressure of 130 and 160 kPa. For PCL Type B, we observed repeatable pore geometry, inter-layer morphology (inset) at 5 mm/s print speed, 180^0C temperature, 225 kPa air pressure, 20% porosity, and 35^0C bed temperature. However, we did not get a repeatable sharp corner. With PCL Type C, we observed repeatable pore geometry, inter-layer morphology (inset), sharp corner, and subsequently a good structure-preserving geometric detail at 2 mm/s print speed, 200^0C temperature, 360 kPa air pressure, 30% porosity, and 40^0C bed temperature. Results are shown in Figure 4. We explored more with PCL Type C to use it for the rest of the paper. In the future, we will continue exploring to fine-tune these process parameters to fabricate acceptable 3D structures ensuring geometric details such as well-defined and consistent macro-porosity with all three types of PCL.

Mn 45000	PCL type A 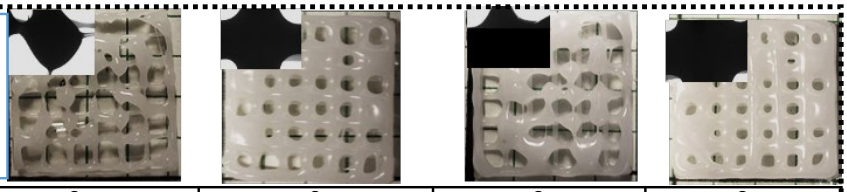			
Print speed (mm/s)	2	2	2	2
Nozzle temp (^{0}C)	100	120	100	120
Print pressure (kPa)	130	130	160	160
Porosity (%)	30	30	30	30
Bed temp (^{0}C)	40	40	40	40
Mn 50000	PCL type B 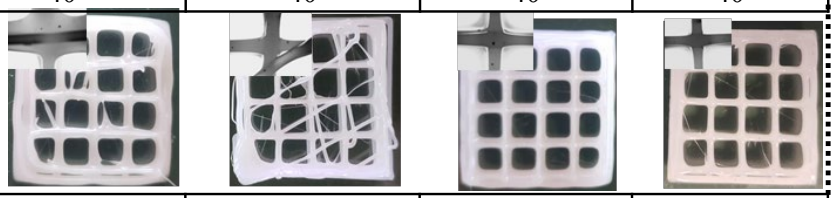			
Print speed (mm/s)	5	5	5	5
Nozzle temp (^{0}C)	180	180	180	180
Print pressure (kPa)	225	225	225	225
Porosity (%)	20	20	20	20
Bed temp (^{0}C)	50	0	40	35
Mn 80000	PCL type C 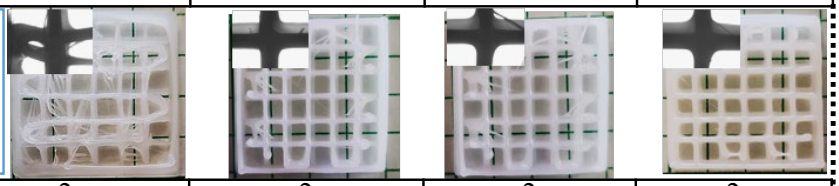			
Print speed (mm/s)	2	2	2	2
Nozzle temp (^{0}C)	180	200	180	200
Print pressure (kPa)	310	310	360	360
Porosity (%)	30	30	30	30
Bed temp (^{0}C)	40	40	40	40

Figure 4: Optimization of process parameters for various PCL used in this research. various factors such as print speed, nozzle, bed temperature, print pressure, and infill percentage were considered to optimize various PCL to use in the next steps. The comparison took place in terms of filament width and pore geometry.

Filament fabrication with PCL

A set of single-layer filaments was fabricated using Type C-PCL pallets with respect to various nozzle temperatures and applied pressures as shown in Figure 5. A constant, 40^0

C bed temperature was maintained during the extrusion process. From Figure 5, with increasing the applied pressure (P), the filament width (FW) increased with an interception of 0.3 and a slope of 0.0013. Result showed 29%, 45%, 62%, 78%, and 107% change of filament width at 160kPa, 220kPa, 280kPa, 340kPa, and 400kPa air pressure respectively. Nozzle temperature 190-2000C was used to extrude the single-layer filament. Morphologically, uniform, and better filament geometry was observed for 340kPa, and 400kPa air pressure. Therefore, we planned to use applied pressure starting from 340 kPa. However, to confirm its performance, we printed scaffolds having uniform pore geometry in the next section.

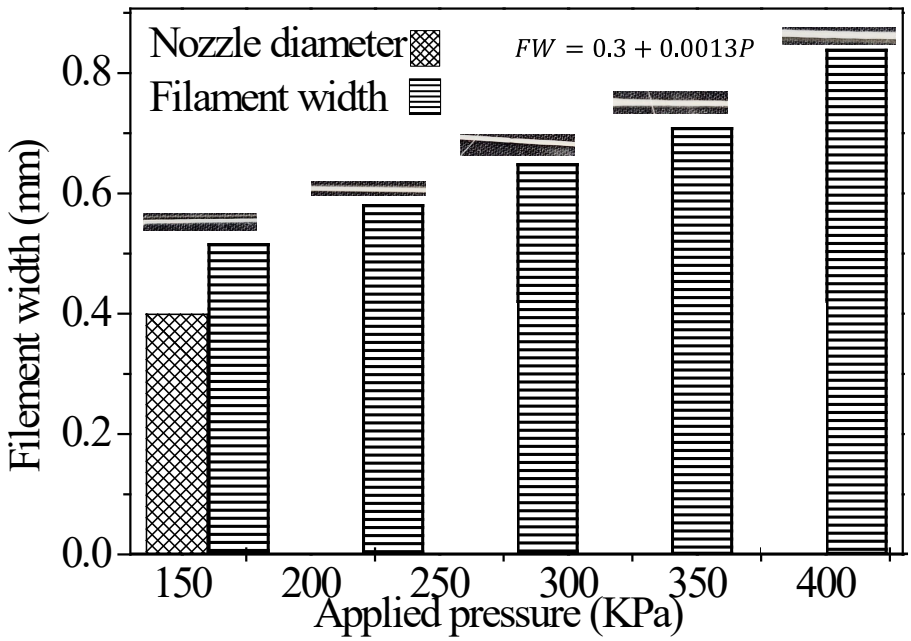

Figure 5: A set of filaments fabricated with a combination of various nozzle temperatures and applied pressure.

Scaffolds fabrication with PCL Type C

To further fine-tune the process parameters, a total of 16 scaffolds having a dimension of 20mm × 20mm × 1mm was fabricated with various printing process parameters such as printing temperatures of 170^{0}C, 180^{0}C, 190^{0}C, and 200^{0}C and applied pressure of 320kPa, 340kPa, 360kPa, and 380kPa with a fashion of (170^{0}C, 320kPa), (170^{0}C, 340kPa) as shown in Figure 6 (a). A 3D surface plot of printability with respect to printing temperature and the applied pressure is shown in Figure 6(b). It is clear from Figure 6(b) that with increasing the printing temperature and applied pressure, a defined pore geometry was observed.

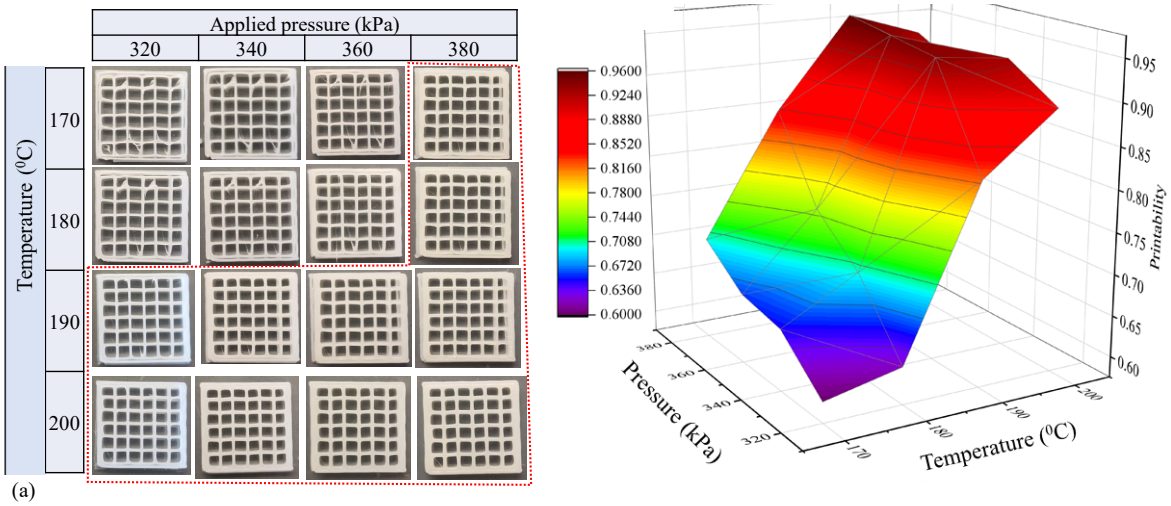

Figure 6: (a) Scaffolds with uniform pore size and geometry with various nozzle temperatures and applied pressure, (b) Optimum temperature and applied pressure combination for better printability.

A range of 0.8-1.0 printability was determined for various temperature and pressure combinations starting from (170^{0}C, 380kPa). However, higher pressure resulted in over-deposition. Therefore, for the rest of the paper, we used a range of applied pressure of 340 KPa to 360 KPa to ensure having continuous filaments with uniform

geometry to support the forthcoming hybrid hydrogel layers. In the future, we will continue exploring to fine-tune these process parameters to fabricate acceptable 3D structures ensuring geometric details such as well-defined and consistent macro-porosity with different types of PCL having various molecular weights.

Mechanical properties of PCL Type C

Compressive stress

Four scaffolds having a dimension of 17×17×3 (mm^3) was fabricated using Type C PCL with process parameters of 2mm/s print speed, 200^0C nozzle temperature, 360 kPa air pressure, 30% porosity, and 40^0C bed temperature as shown in the inset of Figure 7.

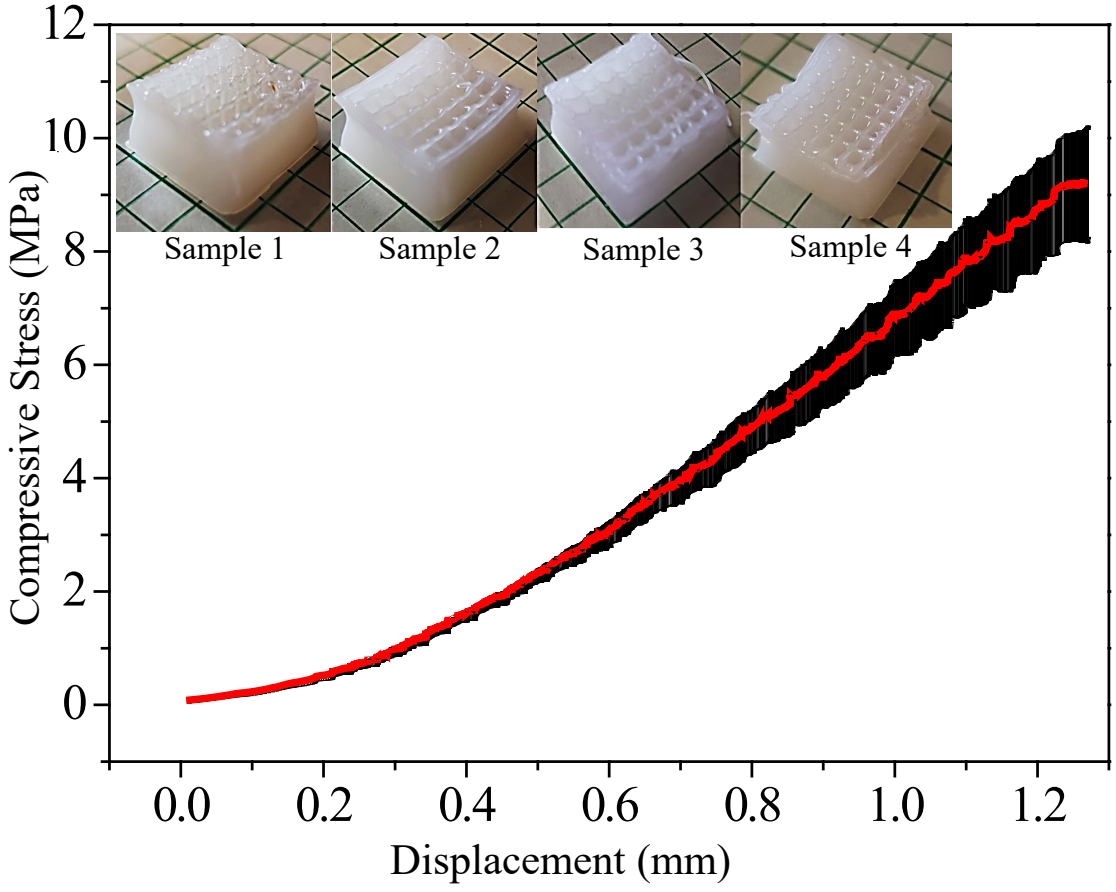

Figure 7: Compressive stress for scaffolds fabricated with Type C PCL. Data is represented in a fashion of mean (red line) ± standard deviation (black shed). Total four sample scaffolds were fabricated and tested to present the repeatability.

This figure demonstrates the capability to fabricate a large structure of Type C PCL ensuring geometric fidelity. The graph represents the compressive stress with respect to the displacement that happened by the applied force for 1 minute. The graph showed an increasing trend of compressive stress with respect to displacement. For example, it showed almost 9.3±0.98 MPa compressive stress at a displacement of 1.27 mm.

Tensile strength

The tension specimens (ASTM D638) were tested in batches of three printed. Force, displacement, and strain (the material stretches) were measured to graphically display the strain-stress curve as shown in Figure 8 which gave an insight into a myriad of material properties. The yield and ultimate tensile stresses were determined as 18.1 and 32.26 MPa respectively from this curve. The material showed a significant plastic behavior for a stress amount of 1 to 17%.

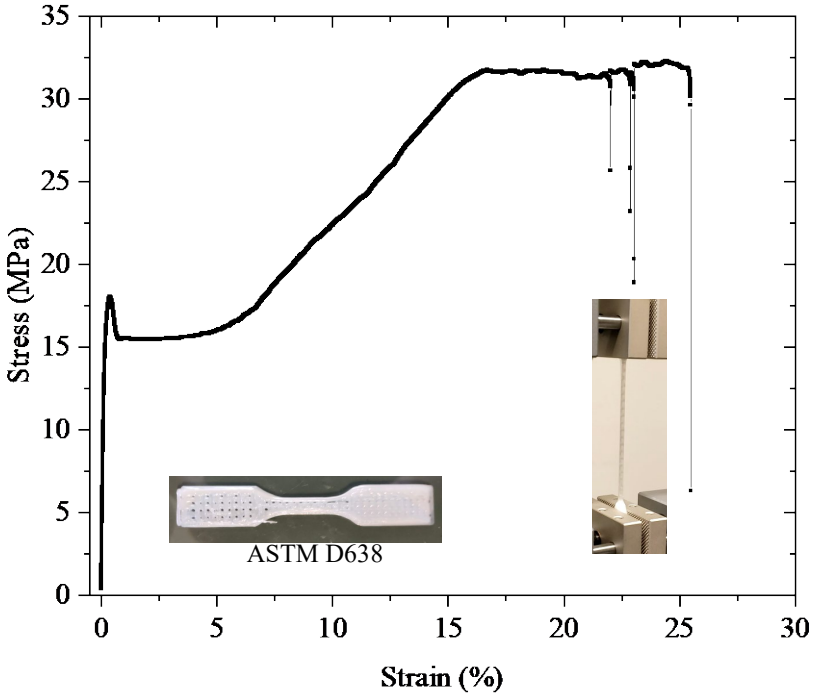

Figure 8: Stress-strain diagram for a dog bone of ASTM D638 sample fabricated with PCL-Type C.

Flow behavior of hybrid hydrogels

The log-log plot of viscosity with respect to the shear strain rate of Type I, Type II, Type III, and Type IV hydrogels are shown in Figure 9. We observed a decreasing trend in the viscosity with the change of the shear rate for all hydrogels. This phenomenon is defined as shear-thinning behavior which is crucial for the extrusion-based bioprinting process [25]. We fitted the viscosity values with the Power-Law Equation ($\eta = K\dot{\gamma}^{n-1}$), where, η is the viscosity, $\dot{\gamma}$ is the shear rate to determine the shear-thinning co-efficient of n and K. Type I, Type II, Type III, and Type IV hydrogels showed various n values such as 0.05, 0.01, and 0.31, 0.05 respectively where K values were 1215000, 4262733, 201450, and 433483 mPa.S^n respectively.

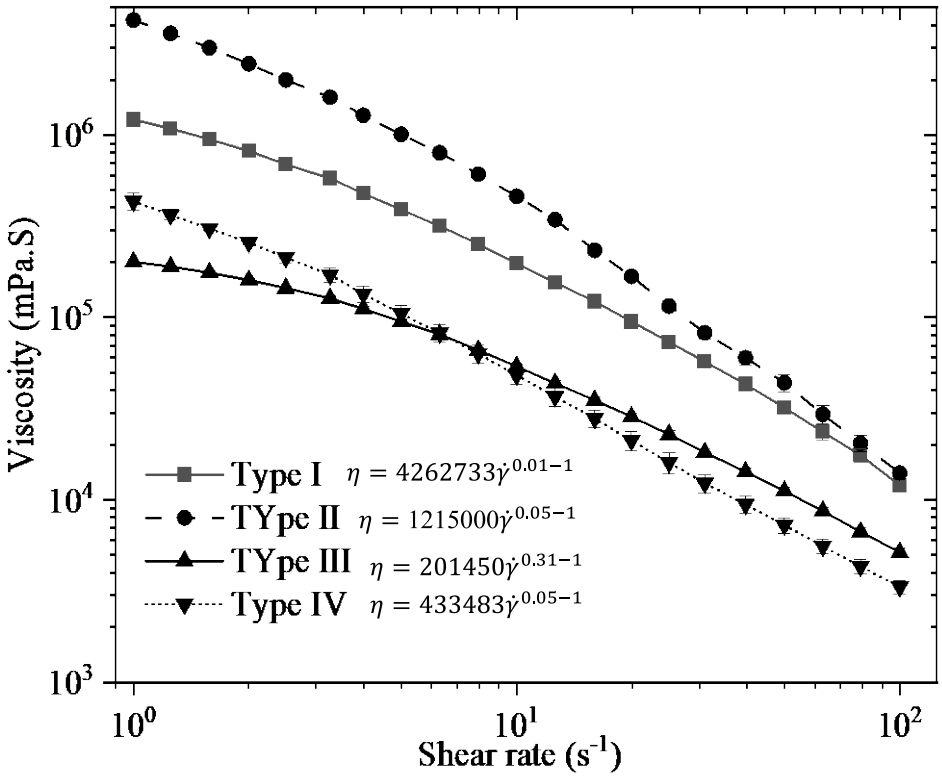

Figure 9: Flow curves for various hybrid hydrogels having various shear thinning factors.

The n and K values confirmed a sequence of viscosity values among those hydrogels, such as Type II>Type I> Type IV >Type III for a range of shear rate from 1-8 s^{-1}. However, it is clear from the graph that, the viscosity of Type-IV is getting reduced at a fast rate compared to Type-III hydrogel after the shear rate of $8s^{-1}$. This phenomenon reflects the better shape holding capacity of Type III at higher shear rate.

High viscous hydrogel experiences more shear stress during extrusion through a nozzle that can adversely affect the encapsulated cells [18]. Since shear-thinning behavior confirms the reduction of viscosity during extrusion, it can help create a protective environment for encapsulated cells in the extrusion-based 3D bioprinting technique. Carboxymethylcellulose (CMC) is commonly used as a viscosity enhancer due to its anionic character. It is composed of β-D-glucose and β-D-glucopyranose-2-O-

(carboxymethyl)-mono-sodium salt. Both of them are connected via β-1,4-glucosidic bonds [26]. Type II hydrogel contained a higher percentage of CMC (6%) compared to Type I (4%) and Type III (2%) which led to a higher viscosity compared to the other two hydrogels. In our recent works, we have explored the viscosities with respect to a range of shear rates from 0.1 to 500 s^{-1} [27] to analyze decreasing trends for a wide range of compositions. In the future, this printing strategy will be utilized for a set of compositions having various viscosities.

Co-printing of PCL and hybrid hydrogels

Shape fidelity of Co-printed PCL and hybrid hydrogels

To determine the geometric fidelity, a set of scaffolds was fabricated using pure PCL, PCL/Type I, PCL/Type II, and PCL/Type III materials. Since the viscosity of Type IV hydrogel was close to Type III hydrogels at a range of shear rate 3-30 (s^{-1}), we did not include Type IV hydrogel for the shape fidelity test. However, it is showing better viscosity with higher shear rate that motivated us to use it for some following experiments. Figure 10 demonstrates the geometry holding capacity of various pores. We considered a set of pores having sizes of 1×1, 2×2, 2×4, and 4×4 (mm2) to analyze the capacity to maintain the geometric fidelity. In this paper, the geometric fidelity of pores was analyzed in terms of printability and diffusion rate of those pores. Figures 11(a) and 11(b) show the printability and diffusion rate of various pores respectively. It is clear from the printability graph that none of the materials was able to create a pore of size 1×1 (mm^2) due to the complete pore closure. All materials expect PCL/Type II showed almost similar printability at a specific pore size, such as 0.95-0.97 at the pore of size 2×2 (mm^2), 1.28-1.42 at the

pore of size 2×4 (mm^2), and 0.94-1.07 at the pore of size 4×4 (mm^2). Since the value of printability depends on the area and perimeter of the actual pore (equation 1) created by layer-upon-layer material deposition, it may not reflect the actual capability to maintain the geometric fidelity all the time. Because actual area and perimeter are directly proportional, it can result in constant printability for various combinations. Therefore, another factor called diffusion rate is readily used which reflects the actual pore closure [28].

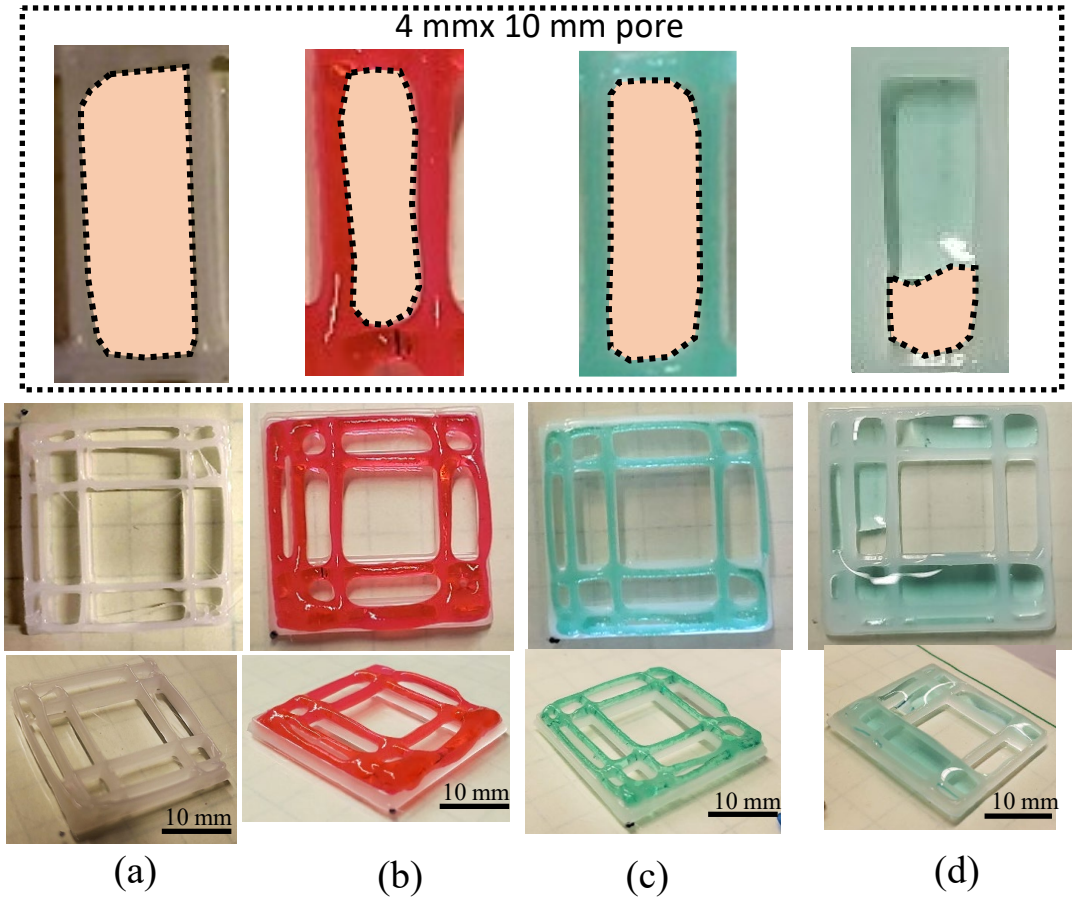

Figure 10: Scaffolds fabricated with natural and synthetic polymers such as (a) PCL Type C, (b) PCL/TYPE I, (b) PCL/TYPE II, and (c) PCL/TYPE III. As an example, the diffusion for

pores having a size of 2 mm × 4mm for PCL Type C, PCL/TYPE I, PCL/TYPE II, and PCL/TYPE III is shown in the box.

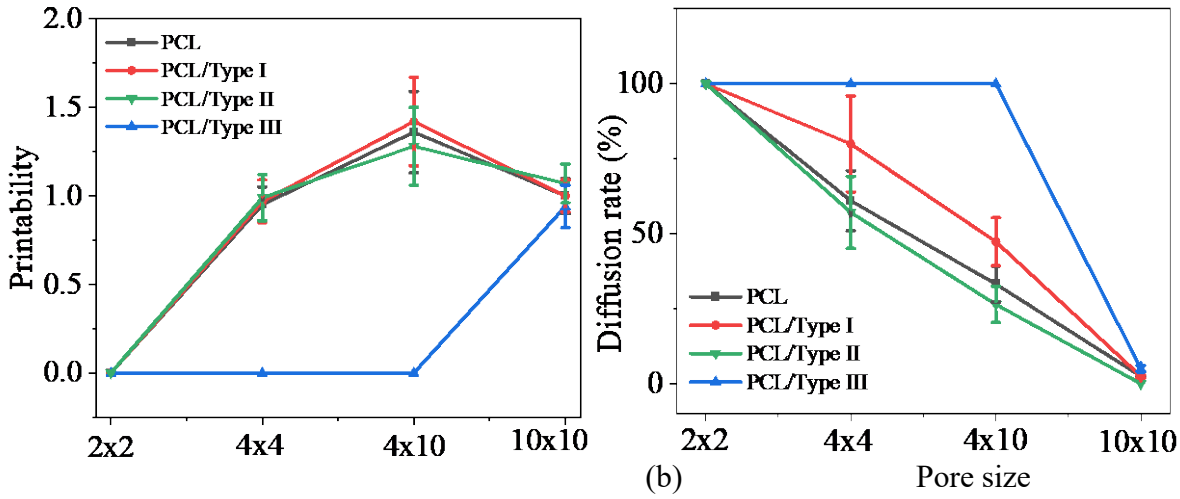

Figure 11: (a) Printability and (b) diffusion rate of scaffolds fabricated with natural and synthetic polymers such as PCL-Type C, PCL/TYPE I, PCL/TYPE II, and PCL/TYPE III simultaneously.

Figure 10 shows co-printed scaffolds with PCL and Type I, Type II, and Type III hydrogels respectively. It is clear from those figures that with increasing the uniform pore area (length × width), the diffusion rate decreased up to 2-5% for a pore of size 4×4 (mm^2). However, among three scaffolds fabricated with natural-synthetic multi-materials i.e., PCL/Type II showed a minimum diffusion rate for all areas of pores because of its higher viscosity.

A defined filament width was observed ensuring minimal deviation with respect to the nozzle diameter. On the other hand, Type III material did not pass to create a distinct pore on PCL which resulted in a 100% diffusion rate for pores of size 1×1, 2×2, and 2×4 (mm^2). A couple of reasons may lead to complete closure of those pores such as lower

viscosity, elevated temperature (32^0C), and lower print speed (4 mm/s). Careful selections of those printing temperature, print speeds, and viscosity may help create acceptable pore geometry with Type III materials. A sequence of viscosity such as Type II> Type I > Type III drives the same sequence of diffusion rate. Various bone and cartilage tissues may need a co-printing of natural and synthetic polymers to ensure patient-specific tissue architecture [11, 29] where this porosity control technique by using various viscous materials can contribute to a successful tissue fabrication.

PCL and with Type I, II, and III hydrogels

A set of scaffolds were fabricated having various toolpath patterns using pure PCL, PCL/Type I, PCL/Type I/Type II, and PCL/Type I/Type II/Type III materials to investigate the capability to fabricate freeform shape with synthetic and low and high viscous hydrogels. Scaffolds pictures are shown in Figure 12. Pure PCL and PCL/Type I maintained the geometric fidelity as designed. However, PCL/Type I/Type III and PCL/Type I/Type II/Type III failed to preserve the defined geometric fidelity. Since, Type III material has the least amount of viscosity compared to Type I and Type II, extruding with the same printing parameters such as 250 μm nozzle diameter, elevated temperature (32^0C), and lower print speed (4mm/s) resulted in an over deposition, and eventually ended up with most of the pore closed. However, the authors believe the systematic selection of those process parameters such as room temperature, high print speed, and smaller nozzle size will help print freeform scaffolds ensuring defined geometry with Type III material.

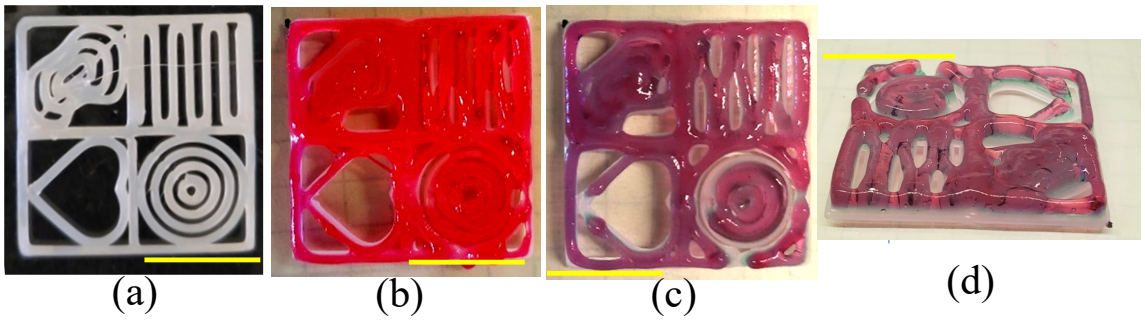

Figure 12: Fabricated scaffolds with various internal architectures. Scaffolds were fabricated with a series of combinations of PCL and hydrogels such as with: (a) pure PCL, (b) PCL and TYPE I hydrogel, (c) PCL, TYPE I, and TYPE II hydrogels, and (d) PCL, TYPE I, TYPE II, and TYPE III hydrogels. Scale bar = 10 mm.

Deposition of hybrid hydrogels on PCL base

Two scaffolds having uniform and non-uniform pore sizes and geometries were fabricated using Type IV hydrogels on a PCL base. PCL base was built with six layers. Four layers of Type-IV hydrogel were deposited on that PCL-based. We observed a 5.5% volumetric shrinkage of the six layers PCL base after printing. For the uniform pore size and geometry, as shown in Figure 13(b), we observed a minimal diffusion rate with a range of 2-5%. However, for various sizes and geometries of pores, pores with smaller sizes such as 1-2 mm, closed completely due to the diffusion as shown in Figure 13(e). Therefore, it is clear that a systemic selection of pore sizes and geometries can produce a defined scaffolds on the PCL base.

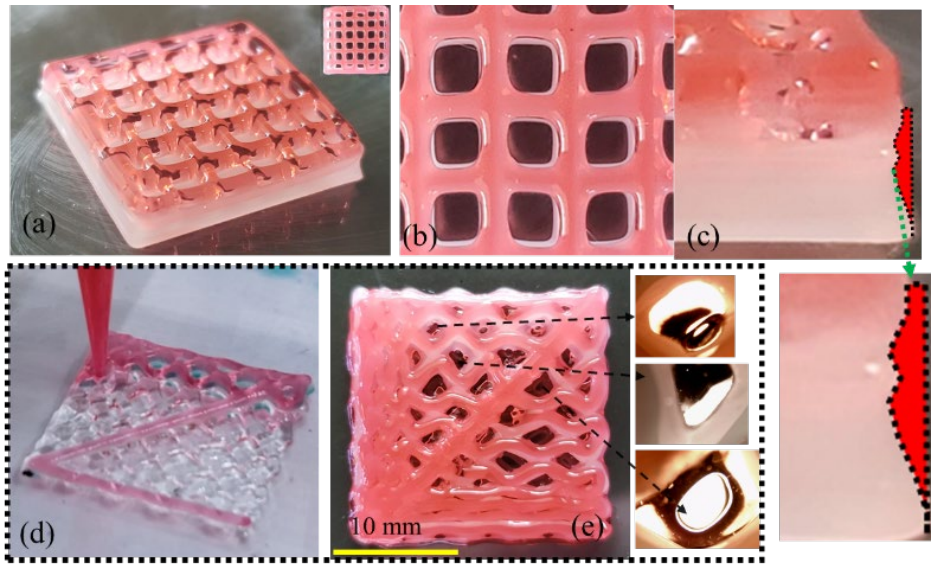

Figure 13: (a, d) Scaffolds fabricated with Type II hydrogels on PCL base, (b) Pore geometry on PCL base, (c) Volumetric change due to shrinkage of PCL, and (e) Various pore sizes and geometries of the scaffold.

Deposition of hybrid hydrogels and PCL alternatively

Scaffold with uniform pore size and geometry was fabricated following an alternating deposition pattern of PCL and Type IV hydrogel as shown in Figure 14 (a). The first layer was fabricated with PCL. The scaffold was fabricated with a total of 10 layers having five layers of PCL and five layers of Type IV hydrogel. We observed a minimal diffusion rate with a range of 2-5% even with this alternating deposition pattern. However, a total of 15% reduced layer height was observed due to the interlayer diffusion between PCL and hydrogel. This indicates a systemic selection of process parameters, and several layers can produce a defined geometry of the scaffold.

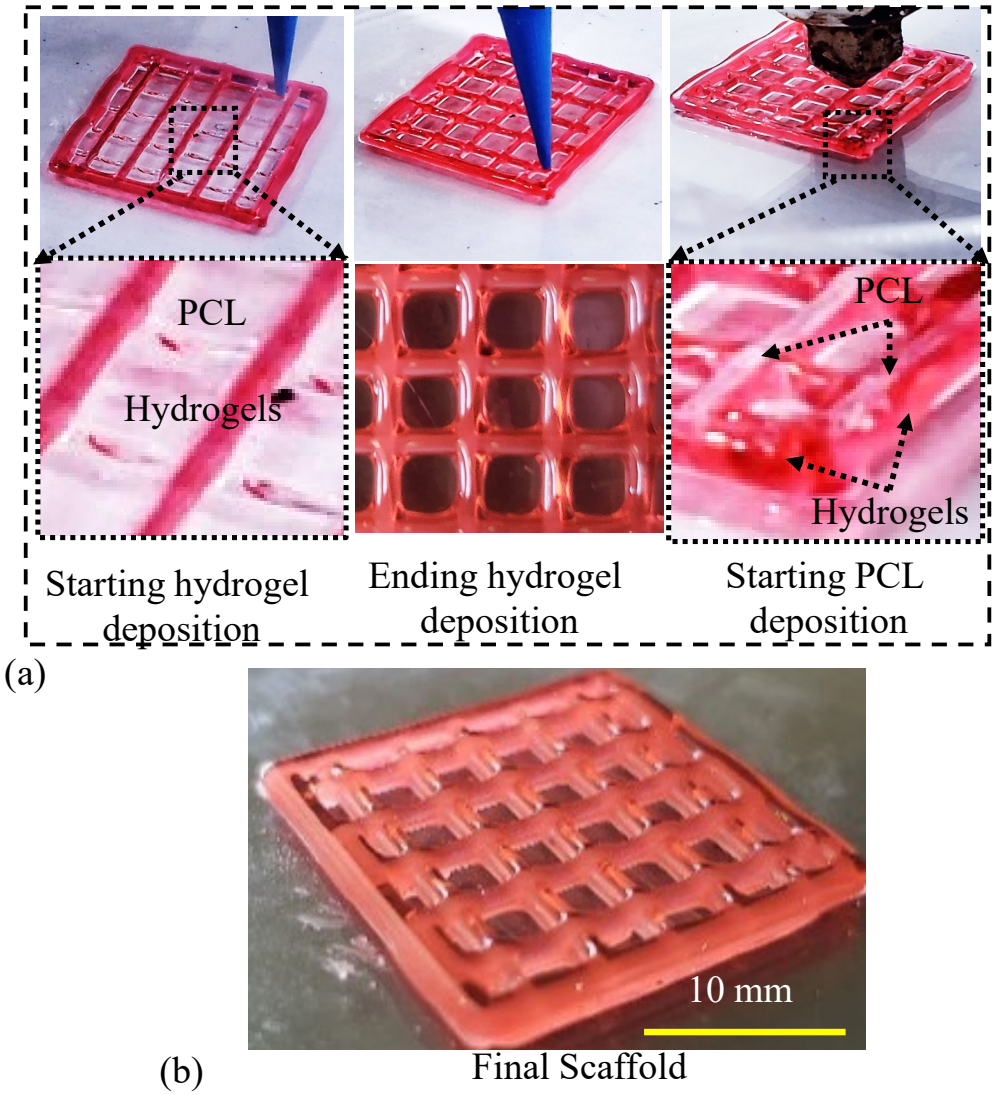

Figure 14: (a) Sequence of alternatively fabricated scaffold with PCL and Type II hydrogel, (c) Final scaffold fabricated by alternatively depositing PCL and Type II hydrogel.

Deposition of PCL as an outer shell and hybrid hydrogels as infill

Two different models such as a circular and a portion of femur models were fabricated with PCL as outer shell Type II and Type IV hydrogels as infill as shown in Figures 15(a) and 15(c) respectively. The defined interaction between PCL and hydrogels and the intersection of hydrogel filaments were observed microscopically as shown in Figure 15(b)

after the fabrication. This reflects the capability to maintain defined geometry of the co-printed scaffolds by PCL and Type II and Type IV hydrogels. The fabricated scaffold left open air to be dried for 30 days to observe the interaction between PCL and hydrogel. While no chemical teste was conducted to measure the interaction between PCL and hydrogel, it was observed that the dried infill hydrogel filament was still connected to the PCL boundary after even 30 days. It is clear from Figure 16 that selecting hydrogel without considering proper viscosity can hinder the defined internal porosity, and eventually the overall shape fidelity of the printed construct. In the future, the source such as ionic interaction, hydrogen bond, electrostatic repulsion, and amount of interaction force between PCL and hydrogels will be determined by rheological and swelling tests [30].

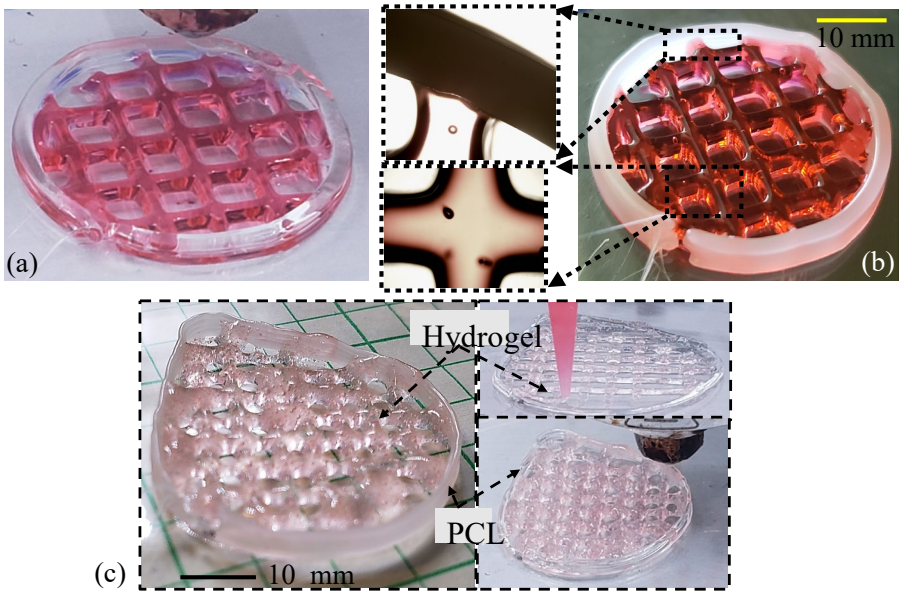

Figure 15: Scaffolds fabricated with natural and synthetic polymers such as (a) PCL/Type II and (c) PCL/Type IV hydrogel. (b) Microscopic observation of the interaction between PCL and Type II hydrogel and the intersection of Type II hydrogels.

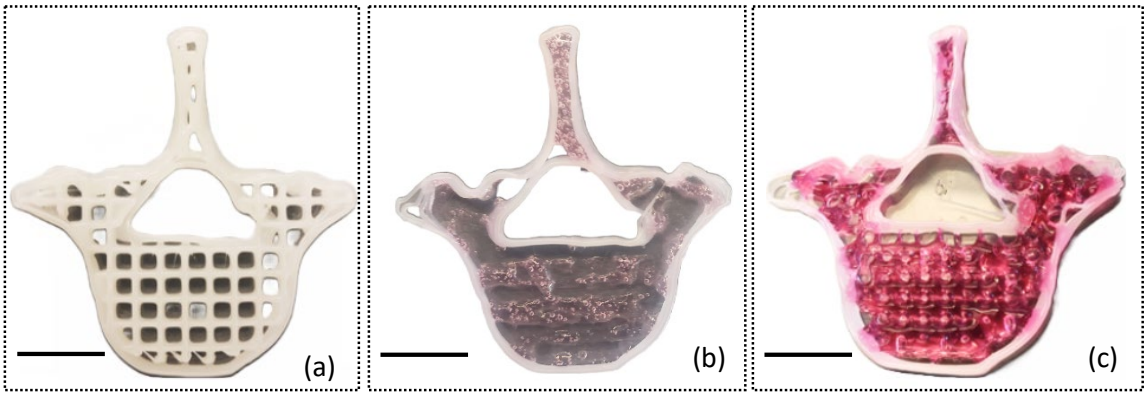

Figure 16: A cross-section of vertebra fabricated with (a) synthetic polymers and (b-c) synthetic and natural polymers with low and high viscous hydrogels. Scale bar = 2 cm.

Controlling filament width varying process parameters

The process parameters can be controlled systematically to obtain the filament with similar width. As a test case, two scaffolds with variational pore size were fabricated with Type-I and Type-II hydrogels with two different sets of process parameters as shown in Figure 17. Process parameters such as layer height, print speed, pressure used to fabricate the scaffold were 0.15mm, 5 mm/s, and 100 kPa respectively for Type-I hydrogel as shown in Figure 17 (a). Since the viscosity of Type-II hydrogel is higher than Type-I hydrogel as shown in Figure 9, to fabricate the same scaffold with Type-II hydrogel as shown in Figure 17 (b) required 10 kPa more pressure i.e., 120 kPa compared to Type-I hydrogel where we maintained other parameters constant. Microscopic view presents only 5% variation of the filament width for scaffolds fabricated with Type-I and Type-II hydrogels. An analytical relationship will be developed including various process parameters to maintain filament width variation for various hydrogels within an acceptable (≤10%) range to confirm the overall geometric fidelity of the scaffold in future.

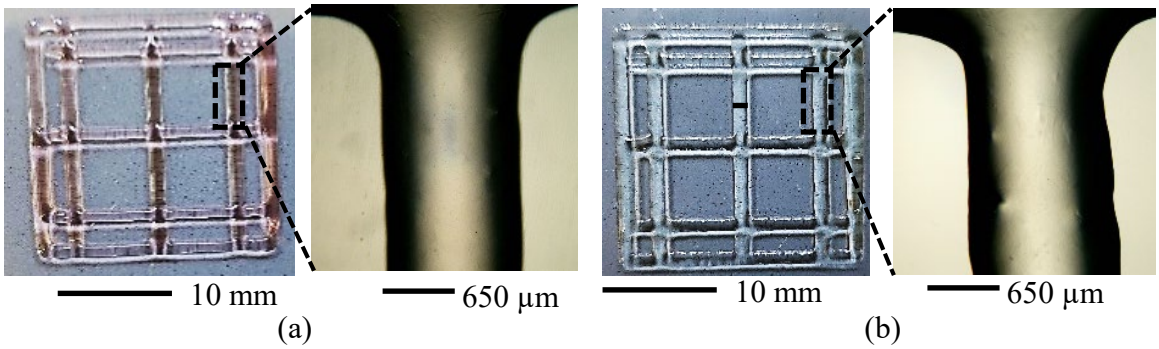

Figure 17: Scaffolds fabricated with (a) Type-I and (b) Type-II hydrogels with two different sets of printing parameters represents similar filament width.

CONCLUSION AND FUTURE WORK

We explored the capacity of fabricating scaffolds co-printed with our already proposed hybrid hydrogels (Type I, Type II, and Type III) and PCL following a set of printing strategies. It is clear from the results that a systematic selection of process parameters can help fabricate a large-scale scaffold with a defined shape fidelity. To define the geometric fidelity of the scaffolds fabricated, we displayed the interplay between optimized PCL and other hybrid hydrogels having low, medium, and high viscosities. As we know, most of the tissues require multiple type of cells to regenerate, this printing strategy can be helpful allowing the extrusion of synthetic and natural biopolymers encapsulating multiple cell types. Moreover, adding synthetic polymers as a part of fabricated tissue scaffolds can assist achieving mechanical integrity, dimensional accuracy, and less time during post-processing. Authors believe fabrication capability of a cell-encapsulated spatially controlled complex heterogeneous 3D scaffold will develop more biomimetic scaffolds capable of replicating the patient-specific tissue architecture

and eventually tissue regeneration. As a part of this effort, we will continue our research to find right kind of material compositions and process parameters suitable for this system. Recently, we published a hybrid pre-crosslinking approach to get better shape fidelity of full-scale scaffolds ensuring internal and external geometries, and conducted a bacterial growth test on pre-crosslinked hydrogels [27]. In future, we will use the same material compositions to extrude to achieve better internal architecture. The cell viability of Type-I and Type-II were assessed in our previous works [16, 18, 31]. Type-I hydrogel was encapsulated with various cell types such as BxPC3 (pancreatic cancer cell), prostate cancer stem cell, and human embryonic kidney (HEK)-293 cell and it showed 92, 91, and 89% cell viability respectively after 15 incubation days [31]. Type-III hydrogel was encapsulated with Porc1 cell, and it showed around 90% cell viability after 10 incubation days. Those results motivated us to use Type-I and Type-III hydrogel as a candidate of high and low viscous hydrogel materials for this paper. Assessing the cell survivability of Type-II hydrogel encapsulating BEAS2B cell lines is our on-going work. We also plan to encapsulate and seed hMSC, other epithelial, and endothelial cell types in our already proposed materials [16, 18, 27] to record the cell actions.

ACKNOWLEDGEMENTS

The research was supported by New Hampshire-EPSCoR through BioMade Award #1757371 from National Science Foundation and New Hampshire-INBRE through an Institutional Development Award (IDeA), P20GM103506, from the National Institute of General Medical Sciences of the NIH.

REFERENCES

[1] C. Mandrycky, Z. Wang, K. Kim and D.-H. Kim, "3D bioprinting for engineering complex tissues," Biotechnology Advances, vol. 34, no. 4, pp. 422-434, 2016/07/01/ 2016, doi: https://doi.org/10.1016/j.biotechadv.2015.12.011.

[2] Y. S. Zhang, K. Yue, J. Aleman, K. Mollazadeh-Moghaddam, S. M. Bakht, J. Yang, W. Jia, V. Dell'Erba, P. Assawes and S. R. Shin, "3D bioprinting for tissue and organ fabrication," Annals of biomedical engineering, vol. 45, no. 1, pp. 148-163, 2017.

[3] J. Malda, J. Visser, F. P. Melchels, T. Jüngst, W. E. Hennink, W. J. Dhert, J. Groll and D. W. Hutmacher, "25th anniversary article: engineering hydrogels for biofabrication," Advanced materials, vol. 25, no. 36, pp. 5011-5028, 2013.

[4] D. M. Kirchmajer and R. Gorkin Iii, "An overview of the suitability of hydrogel-forming polymers for extrusion-based 3D-printing," Journal of Materials Chemistry B, vol. 3, no. 20, pp. 4105-4117, 2015.

[5] H. Rastin, R. T. Ormsby, G. J. Atkins and D. Losic, "3D Bioprinting of Methylcellulose/Gelatin-Methacryloyl (MC/GelMA) Bioink with High Shape Integrity," ACS Applied Bio Materials, vol. 3, no. 3, pp. 1815-1826, 2020.

[6] Y. She, Z. Fan, L. Wang, Y. Li, W. Sun, H. Tang, L. Zhang, L. Wu, H. Zheng and C. Chen, "3D Printed Biomimetic PCL Scaffold as framework interspersed with collagen for long segment tracheal replacement," Frontiers in cell and developmental biology, p. 33, 2021.

[7] D. W. Hutmacher, T. Schantz, I. Zein, K. W. Ng, S. H. Teoh and K. C. Tan, "Mechanical properties and cell cultural response of polycaprolactone scaffolds designed and fabricated via fused deposition modeling," Journal of Biomedical Materials Research: An Official Journal of The Society for Biomaterials, The Japanese Society for Biomaterials, and The Australian Society for Biomaterials and the Korean Society for Biomaterials, vol. 55, no. 2, pp. 203-216, 2001.

[8] A. D. Olubamiji, Z. Izadifar, J. L. Si, D. M. Cooper, B. F. Eames and D. X. Chen, "Modulating mechanical behaviour of 3D-printed cartilage-mimetic PCL scaffolds: influence of molecular weight and pore geometry," Biofabrication, vol. 8, no. 2, p. 025020, 2016.

[9] D. Mondal, M. Griffith and S. S. Venkatraman, "Polycaprolactone-based biomaterials for tissue engineering and drug delivery: Current scenario and challenges," International Journal of Polymeric Materials and Polymeric Biomaterials, vol. 65, no. 5, pp. 255-265, 2016.

[10] M. Raucci, V. D'Antò, V. Guarino, E. Sardella, S. Zeppetelli, P. Favia and L. Ambrosio, "Biomineralized porous composite scaffolds prepared by chemical synthesis for bone tissue regeneration," Acta biomaterialia, vol. 6, no. 10, pp. 4090-4099, 2010.

[11] S. Ramasamy, P. Davoodi, S. Vijayavenkataraman, J. H. Teoh, A. M. Thamizhchelvan, K. S. Robinson, B. Wu, J. Y. Fuh, T. DiColandrea and H. Zhao, "Optimized construction of a full thickness human skin equivalent using 3D bioprinting and a PCL/collagen dermal scaffold," Bioprinting, vol. 21, p. e00123, 2021.

[12] Y. B. Kim, H. Lee, G.-H. Yang, C. H. Choi, D. Lee, H. Hwang, W.-K. Jung, H. Yoon and G. H. Kim, "Mechanically reinforced cell-laden scaffolds formed using alginate-based bioink printed onto the surface of a PCL/alginate mesh structure for regeneration of hard tissue," Journal of colloid and interface science, vol. 461, pp. 359-368, 2016.

[13] L. Ruiz-Cantu, A. Gleadall, C. Faris, J. Segal, K. Shakesheff and J. Yang, "Multi-material 3D bioprinting of porous constructs for cartilage regeneration," Materials Science and Engineering: C, vol. 109, p. 110578, 2020.

[14] A. Zimmerling, Z. Yazdanpanah, D. M. Cooper, J. D. Johnston and X. Chen, "3D printing PCL/nHA bone scaffolds: exploring the influence of material synthesis techniques," Biomaterials Research, vol. 25, no. 1, pp. 1-12, 2021.

[15] F. Koch, O. Thaden, S. Conrad, K. Tröndle, G. Finkenzeller, R. Zengerle, S. Kartmann, S. Zimmermann and P. Koltay, "Mechanical properties of polycaprolactone (PCL) scaffolds for hybrid 3D-bioprinting with alginate-gelatin hydrogel," journal of the mechanical behavior of biomedical materials, vol. 130, p. 105219, 2022.

[16] A. Habib, V. Sathish, S. Mallik and B. Khoda, "3D printability of alginate-carboxymethyl cellulose hydrogel," Materials, vol. 11, no. 3, p. 454, 2018.

[17] M. A. Habib and B. Khoda, "Development of clay based novel bio-ink for 3D bio-printing process," Procedia Manufacturing, vol. 26, pp. 846-856, 2018.

[18] M. Habib and B. Khoda, "Fiber Filled Hybrid Hydrogel for Bio-Manufacturing," Journal of Manufacturing Science and Engineering, pp. 1-38, 2020.

[19] A. Habib and B. Khoda, "Assessing printability of alginate-carboxymethyl cellulose hydrogels," ed: Annual Conference of Institute of Industrial and Systems Engineers, Orlando, Florida, 2018.

[20] O. A. Hamid, H. M. Eltaher, V. Sottile and J. Yang, "3D bioprinting of a stem cell-laden, multi-material tubular composite: An approach for spinal cord repair," Materials Science and Engineering: C, vol. 120, p. 111707, 2021.

[21] C. Nelson, S. Tuladhar and M. A. Habib, "Designing an Interchangeable Multi-Material Nozzle System for 3D Bioprinting Process," in International Manufacturing Science and Engineering Conference, 2021, vol. 85062: American Society of Mechanical Engineers, p. V001T03A005.

[22] L. K. Narayanan, P. Huebner, M. B. Fisher, J. T. Spang, B. Starly and R. A. Shirwaiker, "3D-bioprinting of polylactic acid (PLA) nanofiber–alginate hydrogel bioink containing human adipose-derived stem cells," ACS Biomaterials Science & Engineering, vol. 2, no. 10, pp. 1732-1742, 2016.

[23] K. Arcaute, B. Mann and R. Wicker, "Stereolithography of spatially controlled multi-material bioactive poly(ethylene glycol) scaffolds," (in English), Acta Biomaterialia, Article vol. 6, no. 3, pp. 1047-1054, Mar 2010, doi: 10.1016/j.actbio.2009.08.017.

[24] F. Wang, E. B. Tankus, F. Santarella, N. Rohr, N. Sharma, S. Märtin, M. Michalscheck, M. Maintz, S. Cao and F. M. Thieringer, "Fabrication and Characterization of PCL/HA Filament as a 3D Printing Material Using Thermal

Extrusion Technology for Bone Tissue Engineering," Polymers, vol. 14, no. 4, p. 669, 2022.

[25] H. Li, Y. J. Tan, K. F. Leong and L. Li, "3D bioprinting of highly thixotropic alginate/methylcellulose hydrogel with strong interface bonding," ACS applied materials & interfaces, vol. 9, no. 23, pp. 20086-20097, 2017.

[26] Y. Han and L. Wang, "Sodium alginate/carboxymethyl cellulose films containing pyrogallic acid: physical and antibacterial properties," Journal of the Science of Food and Agriculture, vol. 97, no. 4, pp. 1295-1301, 2017.

[27] C. Nelson, S. Tuladhar, L. Launen and M. Habib, "3D Bio-Printability of Hybrid Pre-Crosslinked Hydrogels," International Journal of Molecular Sciences, vol. 22, no. 24, p. 13481, 2021.

[28] A. Ribeiro, M. M. Blokzijl, R. Levato, C. W. Visser, M. Castilho, W. E. Hennink, T. Vermonden and J. Malda, "Assessing bioink shape fidelity to aid material development in 3D bioprinting," Biofabrication, 2017.

[29] Y. She, Z. Fan, L. Wang, Y. Li, W. Sun, H. Tang, L. Zhang, L. Wu, H. Zheng and C. Chen, "3D Printed Biomimetic PCL Scaffold as framework interspersed with collagen for long segment tracheal replacement," Frontiers in cell and developmental biology, vol. 9, p. 33, 2021.

[30] T. Kopač, A. Ručigaj and M. Krajnc, "Effect of polymer-polymer interactions on the flow behavior of some polysaccharide-based hydrogel blends," Carbohydrate polymers, vol. 287, p. 119352, 2022.

[31] M. A. Habib and B. Khoda, "Rheological analysis of bio-ink for 3D bio-printing processes," Journal of Manufacturing Processes, vol. 76, pp. 708-718, 2022.